Proc. Natl. Acad. Sci. USA
Vol. 89, pp. 212–216, January 1992
Biophysics

Magnetic resonance imaging of perfusion using spin inversion of arterial water

(cerebral blood flow/adiabatic fast passage/hypercarbia/rat brain/cold injury)

DONALD S. WILLIAMS*, JOHN A. DETRE†‡, JOHN S. LEIGH†, AND ALAN P. KORETSKY*§

*Pittsburgh Nuclear Magnetic Resonance Center for Biomedical Research, and §Department of Biological Sciences, Carnegie Mellon University, Pittsburgh, PA 15213; and †Metabolic Magnetic Resonance Research Center, Department of Radiology, and ‡Department of Neurology, University of Pennsylvania School of Medicine, Philadelphia, PA 19104

Communicated by Mildred Cohn, September 19, 1991

ABSTRACT **A technique has been developed for proton magnetic resonance imaging (MRI) of perfusion, using water as a freely diffusable tracer, and its application to the measurement of cerebral blood flow (CBF) in the rat is demonstrated. The method involves labeling the inflowing water proton spins in the arterial blood by inverting them continuously at the neck region and observing the effects of inversion on the intensity of brain MRI. Solution to the Bloch equations, modified to include the effects of flow, allows regional perfusion rates to be measured from an image with spin inversion, a control image, and a T_1 image. Continuous spin inversion labeling the arterial blood water was accomplished, using principles of adiabatic fast passage by applying continuous-wave radiofrequency power in the presence of a magnetic field gradient in the direction of arterial flow. In the detection slice used to measure perfusion, whole brain CBF averaged 1.39 ± 0.19 $ml \cdot g^{-1} \cdot min^{-1}$ (mean ± SEM, n = 5). The technique's sensitivity to changes in CBF was measured by using graded hypercarbia, a condition that is known to increase brain perfusion. CBF vs. pCO_2 data yield a best-fit straight line described by CBF ($ml \cdot g^{-1} \cdot min^{-1}$) = 0.052$pCO_2$ (mm Hg) − 0.173, in excellent agreement with values in the literature. Finally, perfusion images of a freeze-injured rat brain have been obtained, demonstrating the technique's ability to detect regional abnormalities in perfusion.**

Adequate blood flow is crucial to the supply of oxygen and nutrients and the removal of waste from tissue; thus its measurement is important for the assessment of tissue viability and function. A number of techniques have been developed for the measurement of tissue perfusion *in vivo*. Traditionally, perfusion measurements have been made with exogenously administered tracers (1), detected by a variety of techniques. These tracers include xenon, detected by radioactivity or computerized tomography (CT) scans (2), and [^{15}O]water and fluoro[^{11}C]methane, detected by positron-emission tomography (PET) (3, 4). Recently, there have been a number of applications of NMR techniques to measure tissue perfusion. The wash-in or wash-out kinetics of exogenously administered NMR-detectable tracers, such as [^{2}H]water (5, 6), [^{19}F]trifluoromethane (7–9), and chelated gadolinium contrast agents (10), have led to measurements of tissue perfusion.

Here we describe an alternative technique for proton magnetic resonance imaging (MRI) of perfusion rates in the brain by using endogenous water as a diffusable tracer. The method involves labeling the water proton nuclear spins in the arterial blood by continuously inverting them in the neck region before they enter the brain. Continuous inversion is accomplished adiabatically, taking advantage of the linear bulk motion of the blood (11). Proton MRI is used to monitor the effects of perfusion delivering the spin-labeled water to the brain. Solutions to the Bloch equations, which describe the time dependence of magnetization, modified to include the effects of flow, allow regional perfusion rates to be calculated from a set of three images. These are an image with spin inversion, a control image, and a T_1 image. We apply this technique to the measurement of rat brain cerebral blood flow (CBF). To assess the technique's sensitivity to changes in perfusion, we have determined CBF under graded hypercarbia, a condition that is known to increase CBF (12). Finally, by generating perfusion images of a freeze-injured rat brain, we demonstrate that the technique can detect abnormalities in regional CBF.

MATERIALS AND METHODS

Animal Preparation. Male Sprague–Dawley rats (200–300 g; Taconic Farms) were anesthetized with 5% halothane, orally intubated, and ventilated on 1% halothane and a 1:1 N_2O/O_2 mixture. A femoral arterial line was used for monitoring blood pressure and to sample blood for blood gas determinations. The core temperature of the rats was maintained at 37 ± 1°C by using a circulating water pad. Arterial pCO_2 was altered by adding various amounts of CO_2 to the ventilator gas mixture up to an arterial pCO_2 of 100 mm Hg (1 mm Hg = 133 Pa). Perfusion images were usually generated for control and two increased levels of CO_2 from each rat. The mean arterial blood pressure was 100–120 mm Hg and typical control values for pCO_2 and pO_2 were 35 and 150 mm Hg, respectively. The nominal velocity of blood in the carotid artery of the rat was determined by measuring the velocity of blood in a 45-cm long polyethylene tube, of the same internal diameter as the carotid artery, placed as a shunt in the carotid artery. The rat brain was injured by cooling a small region of the skull with liquid nitrogen. Sufficient time was allowed after freezing for the affected region to reach normal body temperature.

NMR Methods. Proton MRI was carried out on a Biospec 4.7-T NMR spectrometer with a 40-cm magnet bore equipped with a 15-cm diameter gradient insert (Bruker Instruments, Billerica, MA). A Bruker 7-cm diameter volume coil was used and image parameters were as follows: recovery time (TR) = 2 s, echo time (TE) = 30 ms, field of view (FOV) = 5 cm, slice thickness (SLTH) = 2 mm, and matrix size = 64 × 64. The freeze-injured rat brain images were obtained with TR = 2 s, SLTH = 2 mm, FOV = 5 cm, and a 128 × 128 matrix resolution. Gradients were applied in the imaging sequence so as to eliminate the contribution of flowing spins

The publication costs of this article were defrayed in part by page charge payment. This article must therefore be hereby marked "*advertisement*" in accordance with 18 U.S.C. §1734 solely to indicate this fact.

Abbreviations: AFP, adiabatic fast passage; CBF, cerebral blood flow; MRI, magnetic resonance imaging; TR, recovery time; TE, echo time.

in arteries and veins (≈99% reduction for velocities > 1 $mm \cdot s^{-1}$) while minimally perturbing tissue water.

Inversion of the inflowing spins in the neck of the rat was accomplished by using principles of adiabatic fast passage (AFP) (11), by continuously applying a low-power radiofrequency field in the presence of a magnetic field gradient during the TR period. The condition for AFP to invert spins in this case is $1/T_1, 1/T_2 << (1/H_1)Gv << \gamma H_1$, where T_1 and T_2 are spin–lattice and spin–spin relaxation times, H_1 is the radiofrequency magnetic field strength, G is the magnetic field gradient strength, v is the linear velocity of the flowing spins, and γ is the gyromagnetic ratio for protons. In our experiments, $G = 1.0\ G \cdot cm^{-1}$, $H_1 = 59$ mG, and v in the rat carotid artery was approximately 10 $cm \cdot s^{-1}$ (1 gauss, G, = 0.1 mT). Thus, $\gamma H_1 = 1571\ rad \cdot s^{-1}$ and $Gv/H_1 = 170\ s^{-1}$. In addition, the measured values of $1/T_1$ and $1/T_2$ are approximately 0.59 s^{-1} and 10 s^{-1}, respectively, for arterial blood at 4.7 T (data not shown); therefore, the condition for AFP is easily fulfilled with ample margin for changes in blood velocity in the arteries.

To ensure that the parameters used for adiabatic inversion were optimal for blood velocities found in the rat, the degree of inversion, α, was measured as a function of velocity in a Tygon tube flow phantom (2.25-mm i.d.) of oxygenated rabbit blood. The integrated area under one-dimensional intensity profiles of a 1-cm slice across the flow phantom was used to determine α from the equation $M(t) = M(0)[1 - 2\alpha \exp(-t/T_1)]$, where t is the time taken for the spins to travel from the inversion plane to the observation slice, $M(t)$ and $M(0)$ are the integrated areas of the profiles for the inversion and the control profiles, respectively, and T_1 is the spin–lattice relaxation time for blood (1.34 s).

To obtain a perfusion image, four pairs of images were obtained for each flow measurement with the inversion plane set alternately to the neck region (inversion image) and a plane outside the rat symmetrically opposite to the imaging detection plane (control image). This control ensures that the effects of off-resonance saturation on brain water intensity due to cross-relaxation with macromolecules are properly accounted for (13, ¶). The four images were summed for improved signal-to-noise ratios. T_{1app} values were measured by using a saturation recovery imaging sequence (14) with recovery times of 10, 2, 1.5, 1, and 0.5 s, respectively. T_{1app} images were generated with a monoexponential fit of the saturation recovery image data at each pixel. Perfusion images were generated by using Eq. **9** (see *Theory*) from the image data for the control image, inversion image, the T_{1app} image, and a blood/brain partition coefficient of water of 0.9 $ml \cdot g^{-1}$ (15).

THEORY

The perfusion imaging technique uses water, labeled by inversion of its proton spins, as a diffusable tracer for the determination of brain perfusion rates. The quantity of tracer in the brain is measured through its effect on the nuclear magnetization of water in the brain. In the presence of flow of water into and out of the brain, the Bloch equations for the brain water magnetization can be written as

$$\frac{dM_b(t)}{dt} = \frac{M_b^0 - M_b(t)}{T_1} + fM_a(t) - \frac{f}{\lambda} M_b(t), \qquad [1]$$

¶Zhang, W. G., Williams, D. S., Detre, J. A. & Koretsky, A. P., Tenth Annual Meeting, Society for Magnetic Resonance in Medicine Book of Abstracts, Aug. 12–16, 1991, San Francisco, abstr. 1143.

where f = brain blood flow in $ml \cdot g^{-1} \cdot s^{-1}$; λ = brain/blood partition coefficient for water defined as [(quantity of water/g of brain)/(quantity of water/ml of blood)]; T_1 = spin–lattice relaxation time of brain water in the absence of flow or exchange between blood and brain; M_b = longitudinal or Z magnetization per g of brain tissue; M_b^0 = value of M_b under fully relaxed conditions; and M_a = Z magnetization per ml of arterial blood.

In Eq. **1**, fM_a and fM_b/λ represent the magnetization of the water entering and leaving the brain, respectively. Several assumptions are made to simplify Eq. **1** (see *Discussion*): a well-mixed compartment has been assumed such that the magnetization of spins in the venous outflow is equal to that in the brain tissue so that $fM_v = fM_b/\lambda$, where M_v is the Z magnetization per ml of venous blood. Under fully relaxed conditions for the brain water and arterial blood, inflowing magnetization = outflowing magnetization, thus

$$fM_a^0 = fM_b^0/\lambda. \qquad [2]$$

It is assumed that arterial spins are continuously inverted such that $M_a(t) = -M_a^0$ at all times. If, in addition, $-fM_b^0/\lambda$ is substituted for fM_a in Eq. **1**, then Eq. **1** can be solved for the time dependence of M_b to give

$$M_b(t) = \frac{M_b^0}{1 + \frac{fT_1}{\lambda}} \times \left[\left(1 - \frac{fT_1}{\lambda}\right) + \frac{2fT_1}{\lambda} \exp -t\left(\frac{1}{T_1} + \frac{f}{\lambda}\right)\right]. \qquad [3]$$

Thus, continuous inversion of arterial spins for varying lengths of time, t, and subsequent sampling of M_b results in an exponential decrease in M_b with a time constant, T_{1app}, given by

$$\frac{1}{T_{1app}} = \frac{1}{T_1} + \frac{f}{\lambda}. \qquad [4]$$

In the steady state ($t = \infty$), M_b reaches M_b^{ss} given by

$$M_b^{ss} = M_b^0 \frac{\left(1 - \frac{fT_1}{\lambda}\right)}{\left(1 + \frac{fT_1}{\lambda}\right)}. \qquad [5]$$

Using Eqs. **4** and **5**, the blood flow, f, can be solved to give

$$f = \frac{\lambda}{T_{1app}} \cdot \frac{M_b^0 - M_b^{ss}}{2M_b^{ss}}. \qquad [6]$$

T_{1app}, M_b^0, M_b^{ss}, and λ are all measurable quantities, allowing f to be determined.

The theory may be extended to obtain spatially resolved perfusion maps in a magnetic resonance imaging mode. In this case, the steady state of the inverted spins in the brain, as given by Eq. **3**, may be maintained during imaging time in one of two ways: (*i*) the spins are inverted continuously for a period much longer than T_{1app} followed by a fast (compared to T_{1app}) image, or (*ii*) spins are continuously inverted throughout the recovery period (TR) between phase-encode steps in a conventional imaging sequence. We have used a conventional imaging sequence. Assuming that the arterial spins in the detection plane are replenished with the inverted spins quickly (compared to the recovery time) so that $M_a(t)$

$= -M_a^0$ at all times, then Eq. **1** can be solved for an arbitrary slice selection pulse with tip angle β and an arbitrary TR. For the case when the inversion pulse is on during the entire TR period, the intensity $M_b^{inv}(TR)$ on a pixel-by-pixel basis is given by

$$M_b^{inv}(TR) = M_b^0 \frac{\left(1 - \frac{fT_1}{\lambda}\right)}{\left(1 + \frac{fT_1}{\lambda}\right)} \frac{\left\{1 - \exp - \left[\left(\frac{1}{T_1} + \frac{f}{\lambda}\right)TR\right]\right\}}{\left\{1 - \cos\beta \exp - \left[\left(\frac{1}{T_1} + \frac{f}{\lambda}\right)TR\right]\right\}}. \quad [7]$$

For a control image with the radiofrequency placed outside the brain at control position during the TR period, the image intensity, M_b^{cont}, is given by

$$M_b^{cont}(TR) = M_b^0 \frac{1 - \exp - \left[\left(\frac{1}{T_1} + \frac{f}{\lambda}\right)TR\right]}{1 - \cos\beta \exp - \left[\left(\frac{1}{T_1} + \frac{f}{\lambda}\right)TR\right]}. \quad [8]$$

Eqs. **7** and **8** can be solved for f, the pixel CBF, to give

$$f = \frac{\lambda}{T_{1app}} \frac{M_b^{cont}(TR) - M_b^{inv}(TR)}{2M_b^{cont}(TR)}. \quad [9]$$

Eq. **9** is identical to Eq. **6**, in that a knowledge of the control magnetization, the steady-state magnetization with inversion of arterial spins, T_{1app}, and λ gives CBF. The determination is independent of the tip angle and TR.

The normocarbic CBF for rat brain is about 1 $ml \cdot g^{-1} \cdot min^{-1}$, and the T_1 (a reasonable estimate of T_{1app}) of the rat brain at 200 MHz is 1.7 s, and λ is 0.9 $ml \cdot g^{-1}$ in the brain (15). Substitution of these values into Eq. **9** indicates that there should be a 6.4% fractional decrease in the intensity of a proton image of the brain with arterial spin inversion.

RESULTS

Fig. 1*A* shows one-dimensional intensity profiles of a phantom consisting of a tube of blood flowing at 10 $cm \cdot s^{-1}$ and a tube of stationary blood as a function of the radiofrequency power level for the adiabatic inversion. In this case, the gradient for AFP was 0.5 $G \cdot cm^{-1}$. As the power levels for the radiofrequency are increased, spins in the flowing tube invert without any effect on stationary spins. Above a threshold power, the inversion remains constant. The variation of the degree of inversion as a function of average velocity measured in the flow phantom is shown in Fig. 1*B*. For this experiment, the radiofrequency power level and the gradient were fixed at 59 mG and 1 $G \cdot cm^{-1}$, respectively. There was 90% inversion over a range of flow velocities from 5 to 27 $cm \cdot s^{-1}$. Below 5 $cm \cdot s^{-1}$, the degree of inversion began to fall off because the left-hand side of the AFP condition (see *NMR Methods*) was no longer being satisfied. The perfusion rates may be corrected for incomplete inversion by replacing the factor 2 in the denominator of Eq. **6** by 2α, where α is the degree of inversion. All subsequent calculations of CBF rates have been corrected for a 90% inversion (i.e., $\alpha = 0.9$) based on the phantom results.

Fig. 2*A* shows a coronal image of a rat head indicating the detection plane used to quantitate perfusion and the resonance planes for the adiabatic inversion radiofrequency. The control transverse image is shown in Fig. 2*B*. Fig. 2*C* shows the difference image between control and inversion images for a rat under moderate hypercarbic conditions (pCO_2 = 60 mm Hg). Significant intensity is seen in the brain, representing an average decrease in intensity of 16% due to inversion of arterial spins. This difference is not detectable from images from a dead rat (data not shown), consistent with the idea that perfusion is being measured. Fig. 2*D* shows a typical T_{1app} image obtained from the rat brain and used in the calculation of the quantitative flow map. At 200 MHz T_{1app} is rather

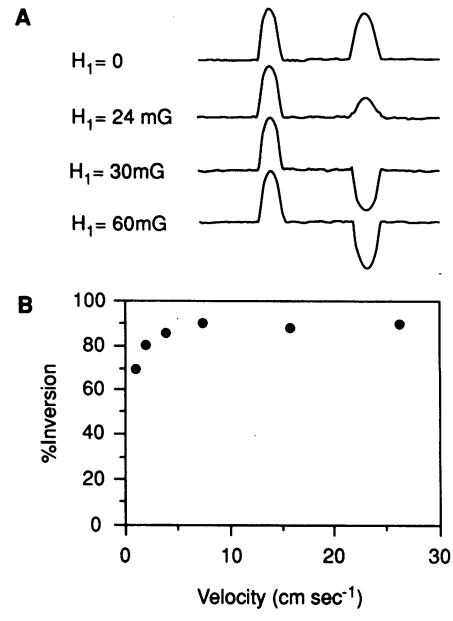

FIG. 1. Phantom studies on the effect of H_1 and velocity on spin inversion by adiabatic fast passage. (*A*) One-dimensional intensity profiles of a phantom consisting of stationary blood (left) and flowing blood (right), respectively, as a function of radiofrequency field strength, H_1, used for inversion. The blood is flowing through a gradient of 0.5 $G \cdot cm^{-1}$. (*B*) Variation of degree of inversion in a phantom of flowing blood as a function of flow velocity. A gradient of 1.0 $G \cdot cm^{-1}$ and H_1 of 59 mG were used for all flow velocities.

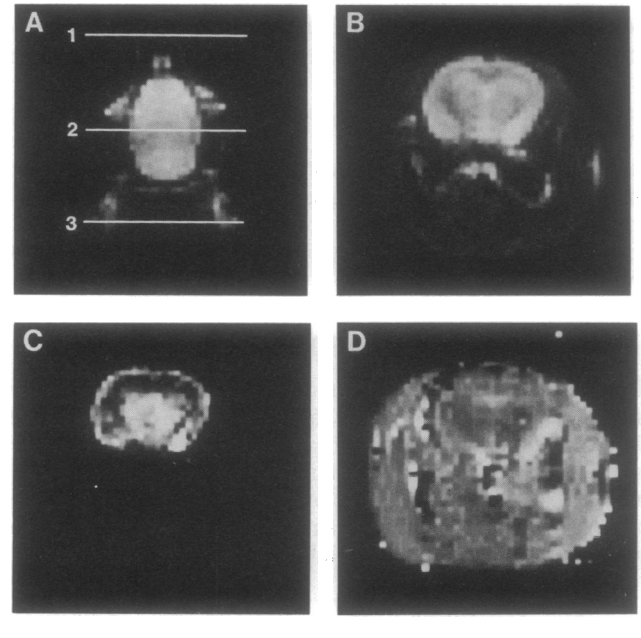

FIG. 2. (*A*) Coronal image of a rat head. The resonance planes for radiofrequency used for spin inversion by AFP for control and inversion images are indicated by 1 and 3, respectively, and plane 2 is the detection plane. (*B*) Control transverse image from the detection plane (plane 2 in *A*). (*C*) Difference image between control and inversion images. (*D*) T_{1app} image.

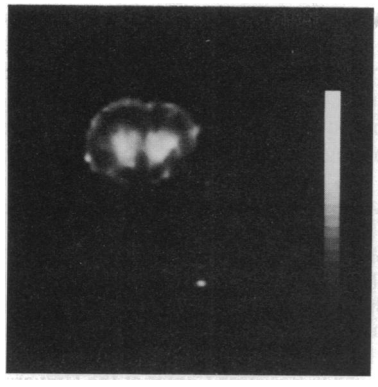

FIG. 3. Perfusion image generated from data shown in Fig. 2. The grey scale is from 0 to 8 $ml \cdot g^{-1} \cdot min^{-1}$.

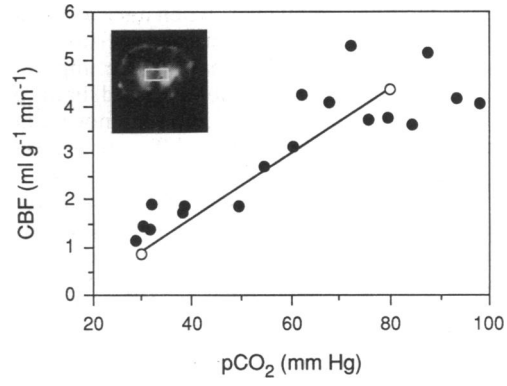

FIG. 4. Response of CBF to graded hypercarbia. The region of the brain used to quantitate flow is indicated by a rectangle in the rat brain perfusion image shown in the *Inset*. ●, CBF measured by arterial spin inversion; ○, data taken from ref. 12, which represent average whole-brain blood flow determined using xenon as a CBF indicator. The solid line is derived from the data in ref. 12.

uniform, with a whole-brain average of 1.5 s and individual pixel values ranging from 1.2 to 2.1 s.

Fig. 3 shows a perfusion image obtained from the data shown in Fig. 2. A three-point smoothing function has been applied to the image. The average whole-brain perfusion rate is 3.0 $ml \cdot g^{-1} \cdot min^{-1}$ for this rat with moderate hypercarbia (pCO_2 = 60 mm Hg). Regional flow rates vary from 1.7 to 6.7 $ml \cdot g^{-1} \cdot min^{-1}$. Increased flow rates are seen in the cortex and deep nuclei, while the dark areas of low flow occur in regions of the rat brain consisting of predominantly white matter.

For normocarbic rats (pCO_2 = 33 ± 1.8 mm Hg), the average brain flow in the detection slice was 1.39 ± 0.19 $ml \cdot g^{-1} \cdot min^{-1}$ (n = 5). This value is in good agreement with previously reported literature values of from 1 to 1.4 $ml \cdot g^{-1} \cdot min^{-1}$ for CBF in rat brain (12, 16, 17). The effects of graded hypercarbia on CBF from the deep nuclei of the brain are shown in Fig. 4. Hypercarbia increased flow in this region of the brain from a control flow of 1.6 ± 0.14 $ml \cdot g^{-1} \cdot min^{-1}$ (mean ± SEM, n = 5) at a pCO_2 of 33 ± 1.8 mm Hg (mean ± SEM, n = 5) to flows of 5.2 $ml \cdot g^{-1} \cdot min^{-1}$ at pCO_2 above 90 mm Hg. The solid line in Fig. 4 is derived from data from Eklof *et al.* (12), who studied the effects of graded hypercarbia on whole rat brain blood flow by using a xenon washout technique. Their data give a relation between CBF and pCO_2 up to 80 mm Hg defined by the equation CBF ($ml \cdot g^{-1} \cdot min^{-1}$) = $0.07pCO_2$ (mm Hg) − 1.26. These data are consistent with Mori *et al.* (17), who measured a 5% change in CBF per mm Hg in pCO_2 (slope = 0.05), using microspheres to measure CBF. The data from our perfusion imaging determination of flow at pCO_2 up to 80 mm Hg yield a best-fit straight line of CBF ($ml \cdot g^{-1} \cdot min^{-1}$) = $0.052pCO_2$ (mm Hg) − 0.173. There is no significant difference ($P > 0.05$) between the slope of this line and the slopes derived from the data from xenon washout or microspheres.

To assess the ability of the perfusion imaging technique to resolve abnormalities in flow, perfusion maps were obtained from a freeze-injured rat brain. Cryogenic lesions have been used to model focal cerebral injury and cause local edema formation (18) and metabolic depression (19). Fig. 5*A* shows a normal T_2-weighted image of the rat brain after freeze injury, where the affected region appears as a bright semicircle in the upper left-hand side of the image due to local edema. Fig. 5*B* shows the calculated flow image in the same slice. There is a region of low intensity corresponding to the injured region. The average flow value in this region is reduced by 70% as compared with the value for a comparable region on the contralateral side of the brain.

DISCUSSION

The growth of MRI as a powerful diagnostic tool has led to much interest in extending the application of MRI to perfusion (5–10). We recently described a steady-state NMR imaging technique for the measurement of tissue perfusion by using endogenous water as a freely diffusable tracer (13). Here, this technique is substantially improved by using adiabatic inversion of blood water spins. The present technique is easier to implement and gives a 2-fold improvement in dynamic range over the earlier saturation technique, allowing increased temporal or spatial resolution. This approach to measuring tissue perfusion is noninvasive and quantifiable and yields flow images with the resolution of MRI. In principle, it can be applied to any organ with a well-defined arterial supply, including heart, liver, and kidney, as well as brain.

Five assumptions have been made to arrive at a regional value of perfusion. First, it has been assumed that water is a freely diffusable tracer. There has been much work which validates the use of labeled ^1H_2O or ^2H_2O as a perfusion tracer (3, 5, 20). At high flow rates, water may not act as a

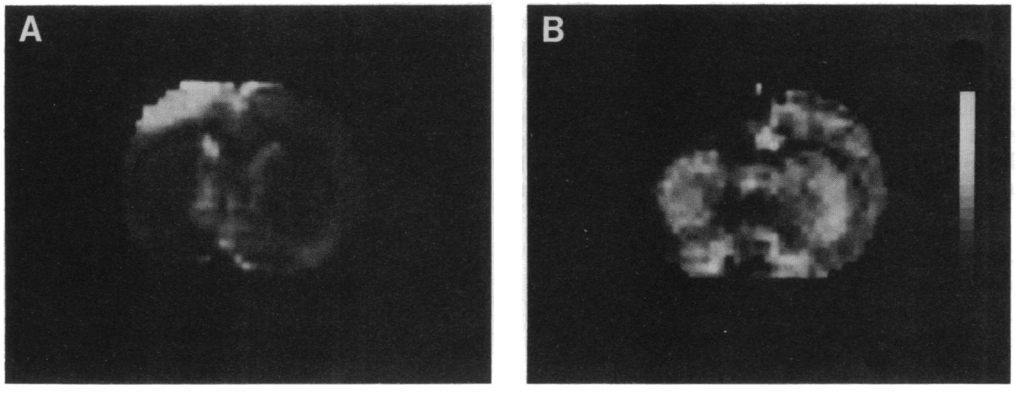

FIG. 5. Comparison of conventional MRI and perfusion imaging of a rat brain subjected to a regional cold injury. (*A*) Conventional T_2-weighted image (TE = 60 ms, TR = 2 s). The injured region shows up as hyperintensity due to a longer T_2. (*B*) Perfusion image of the same slice. The grey scale is from 0 to 6 $ml \cdot g^{-1} \cdot min^{-1}$. The injured region is dark due to low flow.

freely diffusable tracer; however, when a steady state develops, as is the case with this present perfusion imaging technique, diffusion limitations may not be important (20). Second, we assumed a homogeneous blood/brain partition coefficient for water of 0.9 $ml \cdot g^{-1}$. Only minor variations in this value have been measured in different regions of the brain (15). Third, on the basis of phantom studies we assumed that the adiabatic inversion led to 90% inversion of the arterial water spins. The calculated perfusion rates were corrected for incomplete inversion by replacing the factor 2 in the denominator of Eq. **6** by 2α, where α is the degree of inversion (i.e., $\alpha = 0.9$ for 90% inversion). Ultimately, it should be possible to quantitate the amount of arterial inversion by using magnetic resonance angiography techniques (11).

The fourth assumption was that the inverted spins remain inverted until after exchange with tissue water, which means that the arterial transit time must be short compared to the T_1 of blood water. Any relaxation that occurs before exchange would lead to an underestimation of flow directly proportional to the amount of relaxation. On the basis of an arterial flow velocity of 10 $cm \cdot s^{-1}$ from the inversion slice to the base of the brain and a rat brain blood flow of 1 $ml \cdot g^{-1} \cdot min^{-1}$ (12) through an intraarterial volume of 0.6% (21), we estimate that the inverted water spins take a maximum of 460 ms to exchange with tissue water. The amount of relaxation that occurs can be calculated from $M_a = M_a^0[1 - 2\exp(-t/T_1)]$, with $t = 460$ ms and $T_1 = 1.34$ s at 4.7 T. Thus, spins relax approximately 29% before exchanging with tissue water. This calculation accounts for the full length of the capillary bed and should represent a maximum transit time. Preliminary measurements of the transit time for labeled spins to a region of the brain have been made by rapidly sampling magnetization as a function of time after beginning inversion.¶ Values for the transit time between 200 and 400 ms have been measured, indicating that relaxation during the transit time probably has a smaller effect than estimated above. Such measurements can be used to correct the calculated CBF for this effect.¶ Furthermore, the effect of the transit time can be minimized by inverting arterial spins as close to the brain as possible.

The above four assumptions all lead to an underestimation of flow by this perfusion imaging technique. The fact that the value for the CBF measured in the present work agrees with previous measurements using xenon washout (12) and microspheres (17), as does the response of CBF to increasing CO_2, argues that the assumptions made are approximately correct. The spatial pattern of flow measured by the spin inversion perfusion imaging technique is very similar to that measured by blood flow autoradiograms using ^{14}C-labeled iodoantipyrene (22).

The fifth assumption we have made is that inverted spins in the artery do not contribute to the change in signal intensity. The blood arterial content is approximately 0.6% (21), indicating that the contribution of label in the arteries is, on the average, small. In addition, the imaging sequence was designed to eliminate contributions from flowing spins to the signal intensity.

In conclusion, we have demonstrated that spin inversion of arterial water in the neck region causes a measurable effect on the magnetization of water in the brain. This effect can be used to estimate CBF. In combination with standard imaging techniques, a perfusion map can be generated to give a pixel by pixel measurement of CBF. The technique gives values of perfusion in agreement with previous measurement of rat CBF under both normo- and hypercarbic conditions. Finally, regional alterations in perfusion due to cerebral injury can be imaged. It should be possible to extend this perfusion imaging technique to generate perfusion maps of the human brain.

We acknowledge the excellent technical assistance of Maryann Butowicz and thank G. S. Karczmar, Cliff Eskey, I. J. Lowe, and C. Ho for helpful discussions and the use of facilities. This work was supported by National Institutes of Health Regional Resource Grant RR03631 to the Pittsburgh NMR Center for Biomedical Research, National Institutes of Health Regional Resource Grant RR02305, and a grant from the James S. McDonnell Foundation to the Metabolic Magnetic Resonance Research Center at the University of Pennsylvania. We are grateful to the Richard King Mellon Foundation, the Lucille P. Markey Charitable Trust, the Ben Franklin Partnership Program of the Commonwealth of Pennsylvania, and the Ralph M. Parsons Foundation for providing financial support for the establishment of the Pittsburgh NMR Center for Biomedical Research.

1. Kety, S. S. & Schmidt, C. F. (1945) *Am. J. Physiol.* **143**, 53–66.
2. Gur, D., Good, W. F., Wolfson, S. K., Yonas, H. & Shabason, L. (1982) *Science* **215**, 1267–1268.
3. Fox, P. T., Raichle, M. E., Mintun, M. A. & Dence, C. (1988) *Science* **241**, 462–464.
4. Roland, P. E., Eriksson, L., Stone-Elander, S. & Widen, L. (1987) *J. Neurosci.* **7**, 2373–2389.
5. Ackerman, J. J. H., Ewy, C. S., Becker, N. N. & Shalowitz, R. A. (1987) *Proc. Natl. Acad. Sci. USA* **84**, 4099–4104.
6. Detre, J. A., Subramanian, V. H., Mitchell, M. D., Smith, D. S., Kobayashi, A., Zaman, A. & Leigh, J. S. (1990) *Magn. Reson. Med.* **14**, 389–395.
7. Eleff, S. M., Schnall, M. D., Ligetti, L., Osbakken, M., Subramanian, V. H., Chance, B. & Leigh, J. S. (1988) *Magn. Reson. Med.* **7**, 412–424.
8. Ewing, J. R., Branch, C. A., Helpern, J. A., Smith, M. B., Butt, S. M. & Welch, K. M. A. (1989) *Stroke* **20**, 259–267.
9. Detre, J. A., Eskey, C. J. & Koretsky, A. P. (1990) *Magn. Reson. Med.* **15**, 45–57.
10. Belliveau, J. W., Rosen, B. R., Kantor, H. L., Rzedzian, R. R., Kennedy, D. N., Mckinstry, R. C., Vevea, J. M., Cohen, M. S., Pykett, I. L. & Brady, T. J. (1990) *Magn. Reson. Med.* **14**, 538–546.
11. Dixon, W. T., Du, L. N., Faul, D. D., Gado, M. & Rossnick, S. (1986) *Magn. Reson. Med.* **3**, 454–462.
12. Eklof, B., Lassen, N. A., Nilsson, L., Norberg, K., Seisjo, B. K. & Tarloff, P. (1974) *Acta Physiol. Scand.* **91**, 1–10.
13. Detre, J. A., Leigh, J. S., Williams, D. S. & Koretsky, A. P. (1991) *Magn. Reson. Med.*, in press.
14. Fukushima, E. & Roeder, S. B. W. (1981) *Experimental Pulse NMR: A Nuts and Bolts Approach* (Addison-Wesley, London).
15. Herscovitch, P. & Raichle, M. E. (1985) *J. Cereb. Blood Flow Metab.* **5**, 65–69.
16. Nilsson, B. & Sesjo, B. K. (1976) *Acta Physiol. Scand.* **96**, 72–82.
17. Mori, S., Ngai, A. L. C., Ko, K. R. & Winn, H. R. (1986) *Am. J. Physiol.* **250**, H304–H312.
18. Chan, P. H., Longar, S. & Fishman, R. A. (1983) *Brain Res.* **227**, 329–337.
19. Pappins, M. H. (1981) *Ann. Neurol.* **9**, 484–491.
20. Eichling, J. O., Raichle, M. E., Grubb, R. L., Jr., & Ter-Pogossian, M. M. (1974) *Circ. Res.* **35**, 358–364.
21. Hodde, K. C. (1987) in *The Cerebral Veins: An Experimental and Clinical Update*, eds. Aver, C. M. & Loew, F. (Academic, New York), pp. 85–92.
22. Kent, T. A., Quast, M. J., Kaplan, B. J., Lifsey, R. S. & Eisenberg, H. M. (1990) *Magn. Reson. Med.* **13**, 434–443.